

Document downloaded from:

<http://hdl.handle.net/10251/213550>

This paper must be cited as:

Furió-Novejarque, C.; Sala-Mira, I.; Diez, J.; Bondía Company, J. (2024). A model of subcutaneous pramlintide pharmacokinetics and its effect on gastric emptying: Proof-of-concept based on populational data. *Computer Methods and Programs in Biomedicine*. 244. <https://doi.org/10.1016/j.cmpb.2023.107968>



The final publication is available at

<https://doi.org/10.1016/j.cmpb.2023.107968>

Copyright Elsevier

Additional Information

A model of subcutaneous pramlintide pharmacokinetics and its effect on gastric emptying: Proof-of-concept based on populational data

Clara Furió-Novejarque^a, Iván Sala-Mira^a, José-Luis Díez^{a,b} and Jorge Bondía^{a,b,*}

^aInstituto Universitario de Automática e Informática Industrial, Universitat Politècnica de València, C/ Camí de Vera, s/n, València, 46022, Spain

^bCentro de Investigación Biomédica en Red de Diabetes y Enfermedades Metabólicas Asociadas, Instituto de Salud Carlos III, Av. Monforte de Lemos, 3-5. Pabellón 11, Madrid, 28029, Spain

ARTICLE INFO

Keywords:

PK/PD model
Pramlintide
Identification
Type 1 diabetes

ABSTRACT

Pramlintide, an amylin analog, has been coming up as an agent in type 1 diabetes dual-hormone therapies (insulin/pramlintide). Since pramlintide slows down gastric emptying, it allows for easing glucose control and reducing the burden of meal announcements. Pre-clinical *in silico* evaluations are a key step in the development of any closed-loop strategy. However, mathematical models are needed, and pramlintide models in the literature are scarce. This work proposes a proof-of-concept pramlintide model, describing its subcutaneous pharmacokinetics (PK) and its effect on gastric emptying (PD). The model is validated with published populational (clinical) data. The model development is divided into three stages: intravenous PK, subcutaneous PK, and PD modeling. In each stage, a set of model structures are proposed, and their performance is assessed using the Akaike Information Criterion (AIC) and the Bayesian Information Criterion (BIC). In order to evaluate the modulation of the rate of gastric emptying, a literature meal model was used. The final pramlintide model comprises four compartments and a function that modulates gastric emptying depending on plasma pramlintide. Results show an appropriate fit for the data. Some aspects are left as open questions due to the lack of specific data (e.g., the influence of meal composition on the pramlintide effect). Moreover, further validation with individual data is necessary to propose a virtual cohort of patients.

1. Introduction

Amylin is a hormone segregated by the β cells in the pancreas alongside insulin. Its functions include energy expenditure management, inhibition of glucagon secretion, inducing satiation, slowing down gastric emptying, and anti-psychotic effects (Müller et al., 2017). Amylin works in coordination with insulin to regulate glucose after a meal: insulin reduces the amount of glucose in the blood, whereas amylin slows down gastric emptying, delaying the appearance of glucose in plasma. This prevents blood glucose from rising above healthy levels for long periods of time (i.e., hyperglycemia) (Hay et al., 2015).


People with type 1 diabetes (T1D) suffer from the autoimmune destruction of their β cells. The main consequence is that their body fails to produce insulin on its own, so they depend on its external administration through injections or the use of an insulin pump. However, amylin secretion is lost too. Without amylin, gastric emptying does not slow down, aggravating hyperglycemia. This is one of the reasons why managing glucose excursions after a meal remains one of the biggest challenges in T1D therapy (Gingras et al., 2018).

To aid diabetes management, artificial pancreas (AP) systems were developed. These systems consist of a continuous glucose monitor, an insulin pump, and a control algorithm that generates an insulin infusion value depending on the glucose values provided by the monitor. AP's

classic configuration considers insulin as the sole control action. Since insulin has a uni-directional effect, only decreasing glucose values, different configurations that include additional control actions have been developed. In these configurations, insulin is usually accompanied by rescue carbohydrates or glucagon (Wilson et al., 2020; Laugesen et al., 2022; Taleb et al., 2017), which have an opposite effect to insulin. However, pramlintide has been gaining attention as a complement to diabetes therapy (Weinzimer et al., 2012; Ilkowitz et al., 2016; Sherr et al., 2016; Tsoukas et al., 2021a).

Pramlintide is an amylin analog developed around 1995 that has allowed administering amylin externally to counter its absence in people with T1D (Lutz, 2022). Several clinical trials have proved pramlintide's efficacy in reducing postprandial excursions, thus easing glucose control (Kong et al., 1997; Kolterman et al., 1996; Hinshaw et al., 2016). Pramlintide has also been tested in closed-loop trials administered with a fixed ratio with respect to insulin, emulating an insulin-pramlintide co-formulation (Haidar et al., 2020; Tsoukas et al., 2021b). Its main advantage is that it removes the need to provide the algorithm with accurate estimations of the amount of ingested carbohydrates each meal. Clinical trials have proved that using pramlintide, announcing the start time of the meal suffices to provide adequate glucose control (Tsoukas et al., 2021a), alleviating the patients' burden. However, pramlintide dosing is sometimes accompanied by adverse effects such as nausea or vomiting, especially during the first weeks of treatment (Edelman et al., 2007). Hence, new control algorithms need to be investigated to minimize pramlintide infusion and avoid potential side effects.

*Corresponding author

 clafuno@upv.es (C. Furió-Novejarque); ivsami@upv.es (I.

Sala-Mira); jldiez@isa.upv.es (J. Díez); jbondia@isa.upv.es (J. Bondía)

ORCID(s): 0000-0003-2923-6618 (C. Furió-Novejarque);

0000-0002-6228-5190 (I. Sala-Mira); 0000-0002-5659-1212 (J. Díez);

0000-0001-7286-3719 (J. Bondía)

Simulators describing pramlintide and its effect on glucose are essential tools in validating control strategies in a pre-clinical phase. However, there is a lack of simulators that include pramlintide and provide a set of pharmacokinetic (PK) and pharmacodynamic (PD) relations. Pramlintide models in the literature are scarce, the most relevant being Ramkissoon et al. (2014) and Fang et al. (2013). The first incorporates the pramlintide model into a complete glucoregulatory model. However, deriving the effect of pramlintide from plasma glucose measurements can be misleading because there are many agents at play, such as the endogenous glucose production or insulin effect. On the other hand, Fang's model uses data from a previous clinical trial (Colburn et al., 1996) where pramlintide was administered intravenously. As an alternative to PK/PD models, Micheletto et al. (2013) models the effect of pramlintide on the meals by reidentifying the parameters of a meal absorption model. However, parameter sets will be dependent on the pramlintide dose administered. On the other hand, the authors of this work presented a preliminary approach to a new pramlintide model in Miragall et al. (2023).

This work aims to propose a proof-of-concept PK/PD pramlintide model, to be used as a base tool in developing closed-loop control strategies that combine insulin and pramlintide. The model considers subcutaneous administration of pramlintide, as done in an AP system. Intravenous PK data are used to help in the identification process of components of this model. Contrary to Ramkissoon et al. (2014), the PD model will be built from data on the effect of pramlintide over glucose rate of appearance, which describes the changes in glucose only due to meal ingestion. These will allow focusing on how meal effect is modified by pramlintide, without the intervention of other factors such as insulin effect or endogenous glucose production. Amylin has other effects, such as inhibition of glucagon secretion, which are not captured on this model. Hence, the complete amylin PD are not described. However, PD will be used to refer to pramlintide effect on gastric emptying throughout this paper for simplicity. In order to analyze each stage, a literature search was carried out to find suitable data for identification and validation for each of them. A series of model structure hypotheses are then tested using these datasets, and an adequate structure is selected according to the Bayesian Information Criterion (BIC) and Akaike Information Criterion (AIC).

The rest of the paper is organized as follows: Section 2 describes the materials and methods used to develop the model (e.g., datasets, identification procedure, and the model structure selection criteria). Section 3 covers the development of the PK and PD modeling stages. Section 4 presents the final proposed model, and Section 5 lays out the discussion and conclusions of this work.

2. Methods

The development of the proposed pramlintide PK/PD model is divided into three stages: (1) intravenous PK, (2) subcutaneous PK, and (3) PD. The first stage describes

how pramlintide appears in plasma after an intravenous input. The second stage does so from a subcutaneous input, integrating intravenous PK as a submodel. The last stage describes the effect of plasma concentration of pramlintide on gastric emptying. As a result, a subcutaneous pramlintide PK/PD model is produced. This model is integrated with a meal model from literature to test and validate its capabilities. The analysis of each stage is performed separately.

In order to validate the proposed model structures, published clinical data have been gathered across the literature. Parallel to the three stages that compose the model, three kinds of data have been searched for:

- plasma pramlintide concentration after intravenous pramlintide injections,
- plasma pramlintide concentration after subcutaneous pramlintide administration, and
- rate of glucose appearance after a meal accompanied by pramlintide administration.

Unlike other works in the literature (Ramkissoon et al., 2014; Fang et al., 2013), this paper considers the meal rate of glucose appearance rather than glucose values to validate the PD model proposals. Manipulating the rate of glucose appearance allows decoupling the PD pramlintide model from other subsystems in the glucoregulatory model (e.g., insulin effect, endogenous glucose production). However, obtaining the rate of glucose appearance values requires a tracer study, meaning that it is neither trivial nor inexpensive, so only a few works in the literature were found to report this kind of data.

After a thorough literature revision, 17 datasets were selected for this work, described in Table 1. Some other works were discarded because of data undersampling in some periods of interest or lack of data of interest (e.g., only glucose values were reported, which is helpful to observe the effect of pramlintide on glucose but did not provide enough information for our modeling purposes) (Weyer et al., 2003, 2001; Thompson et al., 1996; Rodriguez et al., 2007; Huffman et al., 2009). In every case, mean values are used since no individual curves were available, meaning that the final result is a set of parameters describing pramlintide's average behavior. The same procedure was followed in Ramkissoon et al. (2014). Table 1 provides a summary of the trial protocol followed in each selected work (second column), a description of the data of interest available (third column), and a list of names used as keys to refer to each of the datasets (fourth column). Data points were obtained using the software *WebPlotDigitizer* (Rohatgi, 2022).

The evaluated model structures follow a compartmental model structure. They were implemented as differential equations in Matlab and solved using the `ode45` function. This function uses Runge-Kutta methods to solve the differential equations. The solver applies a variable simulation step size over the total simulation time, which will vary depending on the data.

Table 1

Summary of datasets used for identification and validation in this work.

Source	Trial summary	Data description	Datasets ID
Colburn et al. (1996)	Study evaluating the effect of bolus and infusion administration of pramlintide on 24 men with T1D.	Plasma pramlintide data for 2-minutes boluses (30 μg , 100 μg , 300 μg) and 2-hour infusions (30 μg , 100 μg , 300 μg).	Col-B-30 Col-B-100 Col-B-300 Col-I-30 Col-I-100 Col-I-300
Kong et al. (1998)	Study aimed to observe the effect of single doses of pramlintide on two separate meals. 11 men with T1D participated in the study.	Plasma pramlintide data for boluses (30 μg , 60 μg , 90 μg).	Kon-30 Kon-60 Kon-90
Kolterman et al. (1996)	Effect of pramlintide after accompanying meals with a pramlintide bolus for 14 days on 84 people with T1D.	Plasma pramlintide concentrations on the first study day (30 μg , 100 μg , 300 μg).	Kol-30 Kol-100 Kol-300
Ahrén et al. (2002)	Study of pramlintide and GLP-1 relationship on 9 people with T1D.	Plasma pramlintide concentrations after a 30 μg bolus.	Ahr-30
Chase et al. (2009)	Evaluation of pramlintide PK/PD in 12 adolescents with T1D.	Plasma pramlintide data after pramlintide boluses (30 μg and 15 μg ¹).	Cha-30
Hassan and Heptulla (2009)	Study of pramlintide effect on 8 adolescents with T1D.	Plasma pramlintide data result of a 30 μg pramlintide bolus.	Has-30
Woerle et al. (2008)	Evaluation of pramlintide effect on gastric emptying on 15 people with T1D.	Glucose rate of appearance data (after a meal of 53 g of carbohydrates plus a 30 μg pramlintide bolus or placebo).	Woe-30 Woe-Placebo
Hinshaw et al. (2016)	Study on pramlintide effect on postprandial glucose on 12 people with T1D.	Glucose rate of appearance data (75 g of carbohydrates meal accompanied by 30 μg pramlintide bolus or placebo).	Hin-30 Hin-Placebo

¹The data corresponding to the 15 μg bolus was not used because few data points were available.

The parameters of each proposed model structure were identified to fit the data selected for identification. Parameter values were obtained through an optimization process carried out with Matlab's genetic algorithm (*ga*). This algorithm is population-based and searches randomly across the population, which may avoid providing a solution on a local minimum and finding the global minimum instead.

In each identification, the optimization index was equal to the root mean square error (RMSE) between the data points and the simulation output. The RMSE for each dataset was obtained as follows:

$$\text{RMSE}_d = \sqrt{\frac{1}{N_d} \sum_{i=1}^{N_d} (\hat{y}_i^d - y_i^d)^2} \quad (1)$$

Where d refers to the specific dataset, \hat{y}_i^d are the simulation points, y_i^d are the data points, and N_d is the total number of samples.

The optimization index (J) was calculated as the sum of RMSEs obtained for each set of data used in the optimization process (total number denoted by D):

$$J = \sum_{d=1}^D \text{RMSE}_d \quad (2)$$

When the data within an optimization presented relevant magnitude differences, the normalized RMSE (NRMSE) was used instead of the RMSE.

$$\text{NRMSE}_d = \frac{\text{RMSE}_d}{\max(y^d) - \min(y^d)} \quad (3)$$

The assessment of the model structures was based on the results obtained from the Akaike Information Criterion (AIC) and the Bayesian Information Criterion (BIC). These two metrics commonly serve as selection criteria when proposing different biological models (e.g., van Sloun et al. (2023); Faggionato et al. (2023)). Their formulae are defined as follows:

Table 2

Identification and validation data summary. IV refers to the intravenous pharmacokinetics stage, SC to the subcutaneous pharmacokinetics, and PD, to the pharmacodynamics stage. Datasets keys are defined in Table 1.

Stage	Identification data	Validation data
STAGE-IV1	Col-B-30, Col-B-100, Col-B-300	Col-I-30, Col-I-100, Col-I-300
STAGE-IV2	Col-I-30, Col-I-100, Col-I-300	Col-B-30, Col-B-100, Col-B-300
STAGE-IV3	Col-I-30, Col-B-30, Col-I-100, Col-B-100, Col-I-300, Col-B-300	
STAGE-SC	Kon-30, Kon-60, Kon-90	Kol-30, Kol-100, Kol-300, Ahr-30, Cha-30, Has-30
STAGE-PD0	Woe-Placebo Hin-Placebo	
STAGE-PD1	Woe-30	
STAGE-PD2	Hin-30	

$$AIC = N \cdot \ln\left(\frac{SSR}{N}\right) + 2 \cdot K \quad (4)$$

$$BIC = N \cdot \ln\left(\frac{SSR}{N}\right) + \ln(N) \cdot K \quad (5)$$

In both expressions, N represents the number of data samples, K is the number of parameters in the model, and SSR represents the sum of squared residuals.

$$SSR = \sum (\hat{y}_i - y_i)^2 \quad (6)$$

Table 2 provides an overview of the identifications and validations performed for each stage and the selected data for each purpose. Datasets are listed according to the identifiers defined in Table 1. The first group corresponds to intravenous PK (IV), the second to subcutaneous PK (SC), and the third to PD. More details about each of them will be provided in the following sections.

An identifiability analysis was carried out for each proposed model structure using the Matlab toolbox genSSI (Chiş et al., 2011). This software applies the Generating Series Approach (Walter and Lecourtier, 1982) to determine whether a model is structurally globally identifiable (all the parameters are uniquely determined with the given inputs and output in the absence of noise), structurally locally identifiable (some of the model parameters have a finite set of values), or structurally unidentifiable (at least one parameter has infinite solutions).

3. Model

This section describes the modeling process for each stage, as described in the Methods section. First, the intravenous PK structure will be proposed; second, the subcutaneous PK one; and lastly, the PD model will be addressed.

3.1. Intravenous pharmacokinetics

Intravenous PK describes plasma pramlintide behavior after a pramlintide input is administered directly into plasma. Said input could either be an intravenous injection or the amount of pramlintide coming from the subcutaneous compartments, as it will be later in our case (Section 3.2).

A relevant precedent in literature is the model presented by Clodi et al. (1998). This model comprised a chain of three compartments and was validated using plasma pramlintide clinical data. The trial consisted of a 50 μg pramlintide bolus administration, and nine healthy people participated in the study. Another proposal regarding intravenous PK can be found in Colburn et al. (1996), where a more complex trial was carried out: 24 people with insulin-dependent diabetes mellitus (i.e., T1D) were divided into three groups and were administered 30 μg , 100 μg , or 300 μg , in bolus or infusion form, depending on the study arm. Clodi's model is used in Ramkissoon et al. (2014), with the same parameters used in the original work.

Plasma pramlintide data from Colburn et al. (1996) is used to identify and validate the present proposal (see the first three rows of Table 2). The same dataset was used in Fang et al. (2013) to propose and validate a PK/PD pramlintide model.

In order to best describe pramlintide kinetics, a series of hypotheses have been made, as shown in Table 3. In every row, $U_P(t)$ represents the intravenous pramlintide input and $P(t)$, the concentration of plasma pramlintide. The bottom part of the table lists the evaluated structure combinations, the number of parameters to be identified in each, and whether the combination is structurally globally identifiable.

The first hypothesis (labeled 1) is based upon Clodi's model, following the same model structure. The transfer rates between compartments are identified because the ones in the original work were based on data from people without T1D. Similarly, the second (2) and third (3) proposals reduce the number of compartments needed. A different aspect is also considered: having an extra delay before the compartment where plasma pramlintide is measured (A). Although a delay might not be necessary for intravenous data, since the substance is administered directly to plasma, it was included to account for possible administration delays. Six possible models were considered combining the four model structures as listed in the row "Model combinations" in Table 3.

Since there were plasma pramlintide data for three doses of intravenous boluses and three doses of intravenous infusion, cross-validation was performed, using the bolus data to identify first and validate second, and vice versa with the infusion data (see rows STAGE-IV1 and STAGE-IV2 in Table 2).

Table 3
Evaluated model structures for pramlintide intravenous pharmacokinetics.

ID	Model structure
1	<p>Parameters: $k_e, k_{12}, k_{21}, k_{23}, k_{32}, V_p$</p>
2	<p>Parameters: k_e, k_{12}, k_{21}, V_p</p>
3	<p>Parameters: k_e, V_p</p>
A	<p>Parameters: k_{01}</p>

IV model combinations	1	1A	2	2A	3	3A
Number of parameters	6	7	4	5	2	3
Structurally globally identifiable	✓	V_p, k_{p01} *	✓	✓	✓	✓

*These two parameters were globally identifiable. The rest were all locally identifiable.

The selection of the best model structures for intravenous PK consisted of three steps. First, AIC and BIC values were calculated for validation results in STAGE-IV1. Second, AIC and BIC were calculated for validation in STAGE-IV2 (see row STAGE-IV1 and STAGE-IV2 in Table 8, Appendix A for the results). Then, a combination metric was obtained to integrate the results of both validations. This metric was based on calculating the mean of the means ($\bar{\mu}$) and the median of the medians (\bar{M}), as shown in Equation (7):

$$\bar{\mu}_C = \text{mean}(\mu_{\text{STAGE-IV1}}^C, \mu_{\text{STAGE-IV2}}^C) \quad (7a)$$

$$\bar{M}_C = \text{median}(M_{\text{STAGE-IV1}}^C, M_{\text{STAGE-IV2}}^C) \quad (7b)$$

Variable C represents the criterion considered (either AIC or BIC); μ^C is the mean value of the criterion obtained for STAGE-IV1 or STAGE-IV2; M^C represents the median AIC or BIC value for each stage. The results obtained with these metrics are detailed in Table 8, under the ‘‘Combination of STAGE-IV1 and STAGE-IV2’’ section. Based on these results, the three structures with the lowest index values were selected for the next stage. The selection was not limited to one structure because some were more appropriate to describe infusion behavior, whereas others worked better for bolus data.

Model structures 2, 2A, and 3 consistently provided the three lowest index values, making them the selected structures for this stage. These selected structures are used as the base for evaluating subcutaneous PK models. Since both of the performed identifications (STAGE-IV1 and STAGE-IV2) were focused on either infusion or boluses, we wanted to move forward with a set of parameters for each IV structure that adequately described both behaviors (infusion and boluses). Consequently, using both data collections, a third identification was carried out (STAGE-IV3). The NRMSE is used for calculating J (Equation (2)) in this stage since there is a significant magnitude difference between infusion and bolus data. The resulting parameter values are used for the intravenous PK models in the next stage.

The simulation outputs of the three models after identifying STAGE-IV3 against Colburn data are shown in Figure 1. Note that the models describe the smaller doses (30, 100 μg) better than the largest one, which indicates that the models may not capture certain nonlinearities in the pharmacokinetics. However, the typical doses used in current therapy are closer to 30 μg (see Table 1); hence our interest was to achieve a better description of those doses.

3.2. Subcutaneous pharmacokinetics

Subcutaneous kinetics describes how the drug behaves from the subcutaneous infusion point until the compartment where plasma concentration measurements are taken.

Subcutaneous pramlintide PK models are scarce in the literature. The most relevant precedent is the work in Ramkissoon et al. (2014). In that paper, the authors model intravenous PK with the Clodi model and base the design of subcutaneous PK on previous work focused on testing insulin PK structures (Wilinska et al., 2005).

Similar to the approach followed in the previous section, a series of hypotheses are laid out to test their capability of describing the data. As shown in Table 4, the first assumption (labeled 1) is that just one compartment needs to be added to the intravenous PK model. The second one assumes a chain of two compartments (2). The third also uses two compartments but distributes the flow of pramlintide in a triangular structure (3). The following hypothesis presents two parallel chains (4), assuming a fast and a slow channel in the subcutaneous absorption. Lastly, structure A introduces a bioavailability coefficient to account for some hypothetical loss of pramlintide at the infusion site. The structures are combined to form eight different model candidates (see ‘‘SC

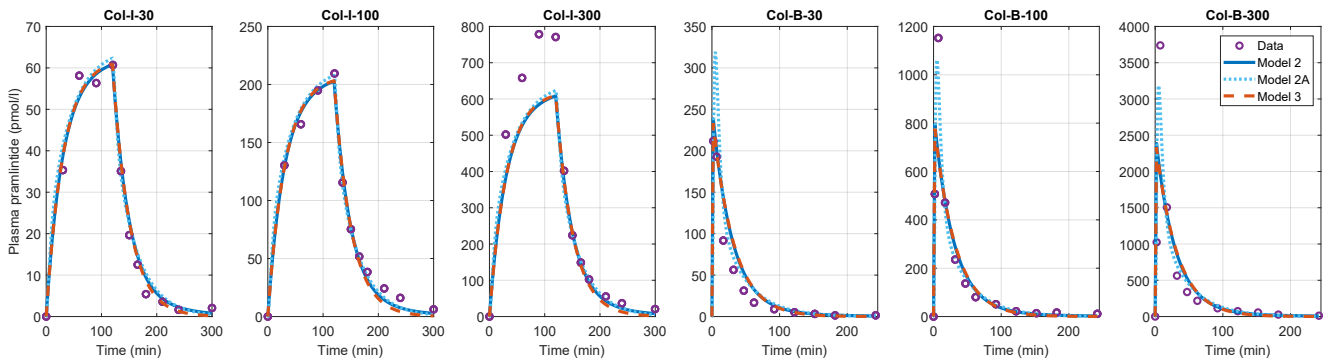


Figure 1: Plasma pramlintide simulation results of identification STAGE-IV3. The three selected intravenous pharmacokinetics structures are identified using data from the six datasets available from Colburn et al. (1996) (30, 100, and 300 μg 2-hour intravenous infusion doses, and 30, 100, and 300 μg 2-min intravenous boluses). The depicted models are used as base models in the subcutaneous pharmacokinetics modeling.

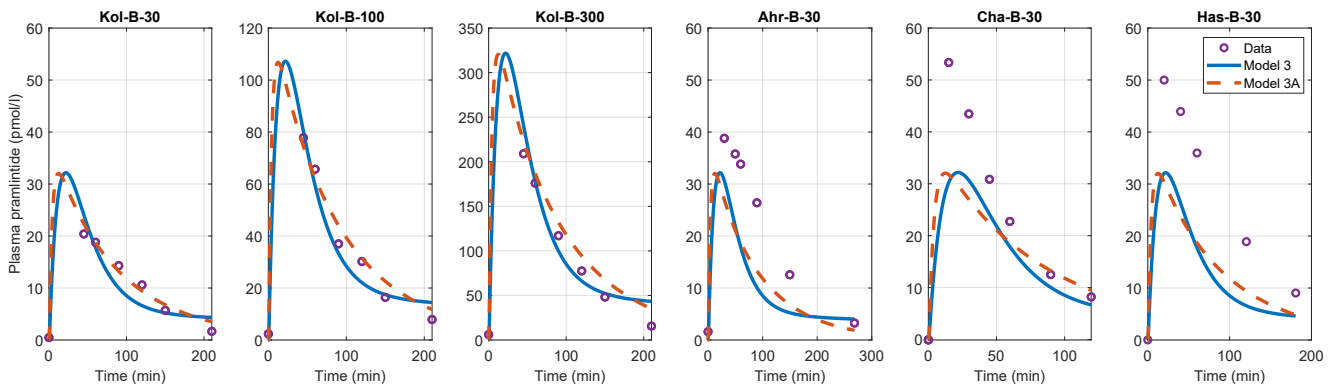


Figure 2: Plasma pramlintide simulation results of the STAGE-SC validation. Validation was performed with a variety of datasets (30, 100, and 300 μg subcutaneous boluses from Kolterman et al. (1996) and 30 μg boluses from Ahrén et al. (2002); Chase et al. (2009); Hassan and Heptulla (2009)).

model combinations” row in Table 4). Each structure was identified three times, using each selected IV structure as the base. Information about the number of parameters for each structure and their structural global identifiability is also included.

Most literature works reporting plasma pramlintide clinical data use subcutaneous boluses. The source works the data was selected from are listed in the second section of Table 1. As detailed in Table 2, the three datasets from Kong et al. (1998) were used for identification, since they captured the concentration peak better than Kolterman et al. (1996), which is undersampled for the initial trial period.

The subcutaneous model combinations were identified three times, using each selected intravenous structure as the base. In order to evaluate these results, AIC and BIC were used, with a modification to account for the number of parameters in the base intravenous model. Parameter K in equations (4) and (5) is substituted by $k + k_{IV}$, where k is the number of parameters in the subcutaneous PK model and k_{IV} is the number of parameters introduced by the intravenous PK model. AIC and BIC values for each identification are included in Table 9, Appendix A.

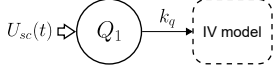

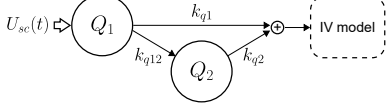
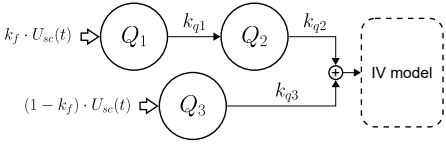
The final model was selected, analyzing the best mean and median AIC and BIC values. The lowest AIC and BIC values were achieved when using intravenous model 3 as the base (see Table 9). In turn, the best AIC and BIC results were produced by subcutaneous models 3 and 3A. Figure 2 shows the output produced by both models. Their behavior is quite similar, but the subcutaneous model 3A fits the tail more accurately, making it the selected model.

The final equations for the PK model, comprised of intravenous submodel 3 and subcutaneous submodel 3A, are presented in Section 4.

3.3. Pharmacodynamics model

Pharmacodynamics describe the effects on the organism of a certain substance in plasma. As the introduction mentions, amylin has many effects, mainly regulated by the central nervous system since amylin receptors are located in the brain (Lutz, 2022). This work focuses on one of amylin’s effects, aiming to define a relationship between the concentration of plasma pramlintide and its effect on the gastric emptying process after a meal.

Table 4
Evaluated model structures for pramlintide subcutaneous pharmacokinetics.

ID	Model structure
1	 <p>Parameters: k_q</p>
2	 <p>Parameters: k_{q1}, k_{q2}</p>
3	 <p>Parameters: k_{q1}, k_{q12}, k_{q2}</p>
4	 <p>Parameters: $k_f, k_{q1}, k_{q2}, k_{q3}$</p>
A	$U_{sc}^a = a_s \cdot U_{sc}$ Parameters: a_s

SC model combinations	1	1A	2	2A	3	3A	4	4A
Number of parameters	1	2	2	3	3	4	4	5
Structurally globally identifiable	✓	✓	✓	✓	✓	L*	✓	✓

*Parameters were all locally identifiable. The analysis could not conclude on structural global identifiability.

Precedents in literature modeling pramlintide PD can be found in Fang et al. (2013), Micheletto et al. (2013), or Ramkissoon et al. (2014). However, the model proposed by Fang et al. (2013) has a main limitation: the pramlintide effect on gastric emptying is independent of the amount of the pramlintide dose. The authors in Micheletto et al. (2013) modify an existing meal model, reidentifying its parameters to fit glucose rate of appearance clinical data (data from Woerle et al. (2008)). However, no new PD model is proposed, and the mechanics to emulate the effect of different pramlintide doses are not described in the paper. The model in Ramkissoon et al. (2014) is a complete PK/PD model that describes the effect of pramlintide modifying the meal action t_{\max} parameter. These modifications are incorporated to the meal model proposed in Hovorka et al. (2004), but they introduce a piecewise function that produces a discontinuity and implementing the model requires an analytical solution of the meal model used.

The pramlintide PD model proposed in this work modifies the glucose rate of appearance after a meal. The meal model used in this work was presented in Dalla Man et al. (2006), and three differential equations describe it (see Table 7 for the description of parameters and values):

$$\frac{dQ_{sto1}(t)}{dt} = U_g(t) - k_{g21} \cdot Q_{sto1}(t) \quad (8a)$$

$$\frac{dQ_{sto2}(t)}{dt} = k_{g21} \cdot Q_{sto1}(t) - k_{empt}(Q_{sto}) \cdot Q_{sto2} \quad (8b)$$

$$\frac{dQ_{gut}(t)}{dt} = k_{empt}(Q_{sto}) \cdot Q_{sto2}(t) - k_{abs} \cdot Q_{gut}(t) \quad (8c)$$

where $Q_{sto}(t)$, $k_{empt}(Q_{sto})$, and α are defined as:

$$Q_{sto}(t) = Q_{sto1} + Q_{sto2} \quad (8d)$$

$$k_{empt}(Q_{sto}) = k_{\min} + \frac{k_{\max} - k_{\min}}{2} \left(\tanh(\alpha \cdot (Q_{sto}(t) - b \cdot D)) + 1 \right) \quad (8e)$$

$$\alpha = \frac{5}{2 \cdot D \cdot (1 - b)} \quad (8f)$$

The system's output is the meal rate of glucose appearance ($R_a(t)$), defined as follows.

$$R_a(t) = \frac{f \cdot k_{abs} \cdot Q_{gut}(t)}{BW} \quad (8g)$$

Of note, $R_a(t)$ in Dalla Man et al. (2006) is defined in mg/kg/min. Hence, the appropriate transformations have been applied to the datasets used in this section to express them in said units.

The proposed model describes the effect of pramlintide on gastric emptying by multiplying the gastric emptying rate, $k_{empt}(Q_{sto})$, by the following function:

$$\eta(\mathcal{P}) = \frac{1}{1 + h(\mathcal{P})} \quad (9)$$

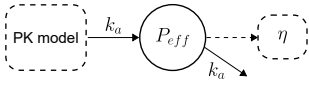
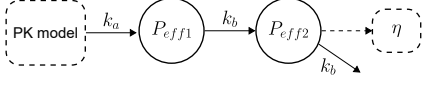
where \mathcal{P} is the input variable to the function, which will be related to the pramlintide concentration, and $h(\mathcal{P})$ is a monotonically increasing function, with $h(0) = 0$, such that the larger the pramlintide concentration is, the slower the gastric emptying.

Similar to the previous sections, a series of structures have been studied to describe pramlintide dynamics. Structures 1 to 3 in Table 5 refer to the definition of \mathcal{P} , whereas structures A to D refer to the form of h .

Structure 1 assumes \mathcal{P} is just equal to the amount of pramlintide in the compartment where plasma pramlintide is measured (P_1). The second structure (2) introduces a delay in the form of an extra compartment. Structure 3 uses a double-compartment chain. On the other hand, function $h(\mathcal{P})$ could be just linear (structure B), be defined by a

Table 5

Evaluated model structures for pramlintide pharmacodynamics.

ID	Model structure
1	$\mathcal{P} = P_1$ Parameters: –
2	 $\mathcal{P} = P_{eff}$ Parameters: k_a
3	 $\mathcal{P} = P_{eff2}$ Parameters: k_a, k_b
A	$h(\mathcal{P}) = \mathcal{P}$ Parameters: –
B	$h(\mathcal{P}) = \alpha \cdot \mathcal{P}$ Parameters: α
C	$h(\mathcal{P}) = \frac{n \cdot \mathcal{P}}{d + \mathcal{P}}$ Parameters: n, d
D	$h(\mathcal{P}) = \frac{n \cdot \mathcal{P}^e}{d^e + \mathcal{P}^e}$ Parameters: n, d, e

PD model combinations	1A	1B	1C	1D	2A	2B
Number of parameters	–	1	2	3	1	2
Globally identifiable	–	✓	✓	✓	✓	✓
PD model combinations	2C	2D	3A	3B	3C	3D
Number of parameters	3	4	2	3	4	5
Structurally globally identifiable	✓	L*	✓	✓	✓	✓

*Parameters were all locally identifiable. The analysis could not conclude on structural global identifiability.

Michaelis-Menten (C), or a Hill equation (D), which are widely used structures to describe saturation in biological processes (Goutelle et al., 2008).

Each of the possible inputs is paired up with each of the possible function forms, as shown in the bottom area of Table 5. Of note, combination 1A introduces no new parameters to be identified, so no identifiability analysis was performed for this structure.

Data on glucose rate of appearance is more scarce in the literature than glucose data. This is due to the complexity of the analysis and infrastructure involved (i.e., triple-tracer study (Basu et al., 2003)). To our knowledge, the only works in the literature that perform this kind of analysis including

Table 6

Meal composition reported in Woerle et al. (2008) and Hinshaw et al. (2016). “D” denotes the number of carbohydrates used as input to the meal model for the simulations carried out in this work.

Dataset	kcal	Carbohydrates	Fat	Protein	D
Woerle	450	45%	30%	25%	53 g
Hinshaw	703.2	55%	30%	15%	75 g

pramlintide were the works by Woerle et al. (2008) and Hinshaw et al. (2016). In both clinical trials, the protocol follows two arms: administering a 30 μg pramlintide dose alongside a meal or a placebo dose. The glucose rate of appearance is reported for both experiments. Placebo datasets were used to identify two distinct sets of parameters for the meal model (identification STAGE-PD0, Table 2), before introducing any pramlintide model. Parameter values are reported in Table 7.

Two different meal model parameters were necessary to describe each placebo dataset because the behavior of the observed signals is noticeably different (see data in Figure 3, upper row). Woerle data reaches a peak value of around 4 mg/kg/min, whereas Hinshaw data doubles that amount. In addition, Woerle data’s disappearance rate has a value of around 160 minutes, whereas, for Hinshaw’s, its value is 100 min, meaning the food leaves the stomach much faster in the second dataset. These discrepancies could be caused by differences in the meal composition (Table 6). For instance, meals reported by Hinshaw et al. (2016) contain more carbohydrate and less protein than those reported by Woerle et al. (2008), which may explain the larger and rapid peak observed in Hinshaw data (Paterson et al., 2015).

However, we also found that a single set of parameters for the pramlintide model could not explain the transformation in both datasets. Some preliminary identifications were carried out as a cross-validation, similar to STAGE-IV1 and STAGE-IV2 (Section 3.1). Nevertheless, the identification of one of the datasets had suboptimal results in the validation performed with the other one. How the pramlintide effect is affected by meal composition is out of the scope of this work since no suitable data is available. Consequently, independent identifications were carried out for each dataset (STAGE-PD1 with Woerle data and STAGE-PD2 with Hinshaw data), aiming to find a common model structure.

All model structures from Table 5 were identified for each dataset. AIC and BIC results are reported in Table 10, Appendix A. Of note, these values refer to identification results as opposed to the previously presented results since no validation data is available for this stage. Results for STAGE-PD1 show that the best structure to fit Woerle data is model 2D. However, for STAGE-PD2, the decision is split between 2D and 1D. Simulation results in Figure 3 (bottom row) show the responses obtained with both proposals. Although their AIC and BIC values are similar, the fit of 2D for Woerle data is closer to the data than model 1D. On the other hand, the results for both structures in Hinshaw data are fairly similar.

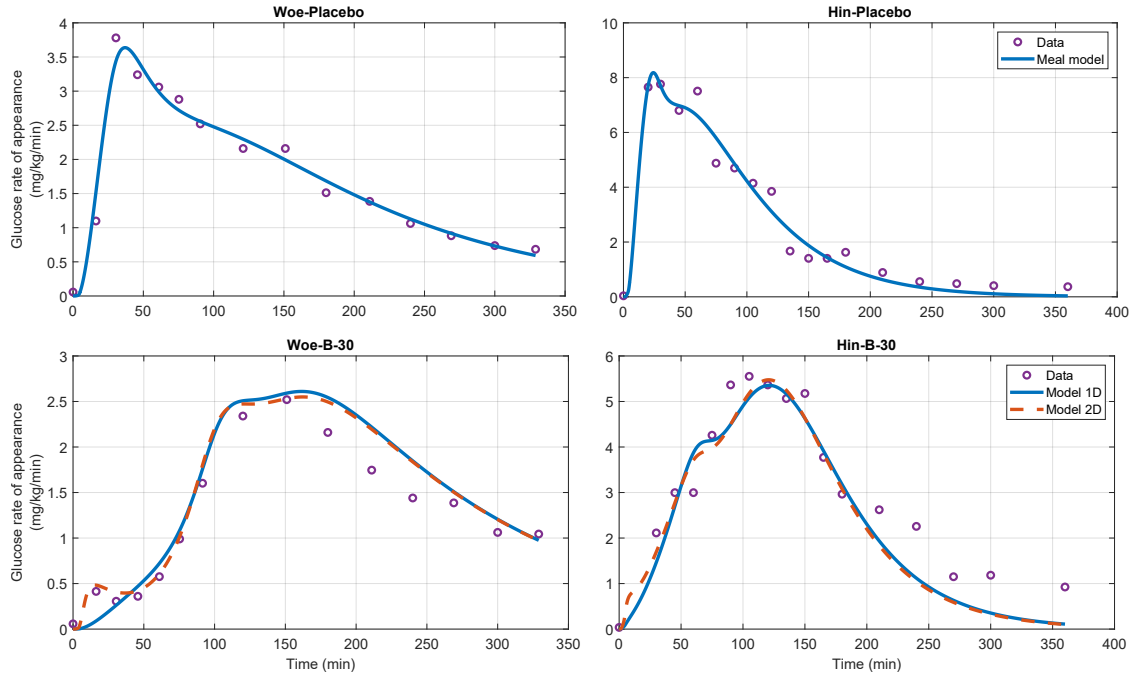


Figure 3: Glucose rate of appearance simulation results. Columns correspond to each dataset used (Woerle et al. (2008) data on the left column, and Hinshaw et al. (2016) on the right column). Upper row shows the meal model identification results for the trial arm of meal + placebo (STAGE-PD0). Bottom row presents the fit of PD model structures 1D and 2D to the meal + pramlintide data (STAGE-PD1 and STAGE-PD2, respectively).

Since our goal is to propose a structure that can adapt to different types of data, our proposed solution will be model 2D.

The behavior difference at the beginning of the simulation of the pramlintide models is mainly introduced by the parameter k_a , which represents the delay introduced by compartment P_{eff} . It symbolizes the time it takes for pramlintide to be effective after its appearance in plasma. In the Woerle dataset, it has a value of around 12 minutes, whereas, for the Hinshaw data, the identified value is around 4 minutes. This allows observing the original glucose rate of appearance in the first samples of the simulation before the pramlintide takes effect and slows down the glucose rise.

4. Final model

Figure 4 presents an overview of the final proposed PK/PD pramlintide model. The equations that conform it are defined next:

$$\frac{dQ_1(t)}{dt} = a_s \cdot U_{sc}(t) - (k_{q1} + k_{q12}) \cdot Q_1(t) \quad (10a)$$

$$\frac{dQ_2(t)}{dt} = k_{q12} \cdot Q_1(t) - k_{q2} \cdot Q_2(t) \quad (10b)$$

$$\frac{dP_1(t)}{dt} = (k_{q1} \cdot Q_1(t) + k_{q2} \cdot Q_2(t)) - k_e \cdot P_1(t) \quad (10c)$$

$$P(t) = \frac{P_1(t)}{V_p} \quad (10d)$$

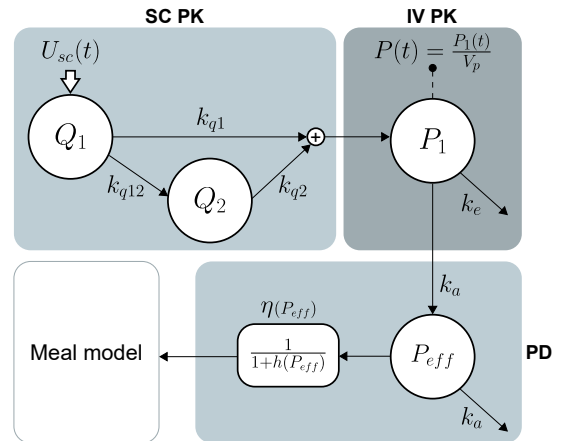


Figure 4: Pramlintide model proposal overview. The three main stages are represented: subcutaneous PK (equations (10a), (10b)), intravenous PK (equation (10c)) and PD (equations (9), (10e), (10f)). The input to the system, $U_{sc}(t)$, is the subcutaneous pramlintide infusion. Pramlintide concentration in plasma is measured as $P(t)$. Pramlintide takes effect by modulating the glucose rate of appearance obtained through a meal model (equations (8)).

$$\frac{dP_{eff}(t)}{dt} = k_a \cdot (P_1(t) - P_{eff}(t)) \quad (10e)$$

$$h(P_{eff}) = \frac{n \cdot P_{eff}^e}{d^e + P_{eff}^e} \quad (10f)$$

Table 7

Pramlintide PK/PD model and meal model signals and parameters' descriptions and values. Meal model and pramlintide PD parameters have two values: the one on the left corresponds to values identified for data from Woerle et al. (2008), and the ones on the right, from Hinshaw et al. (2016).

Symbol	Units	Value	Description
$U_{sq}(t)$	pmol/min	–	Pramlintide subcutaneous infusion
$Q_1(t)$	pmol	–	First subcutaneous compartment
$Q_2(t)$	pmol	–	Second subcutaneous compartment
$P_1(t)$	pmol	–	Plasma pramlintide compartment
$P(t)$	pmol/l	–	Plasma pramlintide volume
$P_{eff}(t)$	pmol	–	Pramlintide effect compartment
a_s	-	0.4235	Pramlintide bioavailability
k_{q1}	min ⁻¹	0.0974	Rate from first subcutaneous compartment to plasma
k_{q12}	min ⁻¹	0.1667	Rate from first to second subcutaneous compartment
k_{q2}	min ⁻¹	0.0109	Rate from second compartment to plasma
k_e	min ⁻¹	0.0322	Output rate from plasma compartment
V_p	l	31.549	Plasma distribution volume
k_a	min ⁻¹	0.0798 0.2671	Rate in the pramlintide effect compartment
n	-	76.662 15.156	Numerator coefficient in Hill equation from $h(P_{eff})$
d	pmol	960.87 908.01	Denominator in Hill equation from $h(P_{eff})$
e	-	4.5363 3.2745	Exponent in Hill equation from $h(P_{eff})$
$U_g(t)$	mg/min	–	Meal input rate
$Q_{sto1}(t)$	mg	–	Solid phase of glucose in the stomach
$Q_{sto2}(t)$	mg	–	Liquid phase of glucose in the stomach
$Q_{gut}(t)$	mg	–	Glucose mass in the intestine
$k_{empt}(Q_{sto})$	min ⁻¹	–	Rate constant of gastric emptying
$R_a(t)$	mg/kg/min	–	Glucose rate of appearance in plasma
D	mg	–	Amount of ingested glucose
f	-	0.9	Fraction of intestinal absorption that appears in plasma
BW	kg	76 86	Body weight
b	%	0.8235 0.8355	Percentage of the dose for which k_{empt} decreases to $(k_{max} - k_{min})/2$
k_{abs}	min ⁻¹	0.0547 0.2280	Rate constant of intestinal absorption
k_{min}	min ⁻¹	0.0074 0.0196	k_{empt} minimum value
k_{max}	min ⁻¹	0.0273 0.0350	k_{empt} maximum value
k_{g21}	min ⁻¹	k_{max}	Grinding rate

Equations (10a) and (10b) correspond to the subcutaneous PK (subcutaneous model 3A). Equation (10c) describes the intravenous kinetics (intravenous model 3), and Equation 10d the plasma pramlintide concentration. Finally, equations (10e) and (10f) represent PD model 2D.

Then, applying function η (Equation (9)) to the meal model, the equations for the states $Q_{sto2}(t)$ and $Q_{gut}(t)$ are modified so that the effect of pramlintide acts on the gastric emptying parameter:

$$\frac{dQ_{sto2}(t)}{dt} = k_{g21} \cdot Q_{sto1}(t) - \eta(P_{eff}) \cdot k_{empt}(Q_{sto}) \cdot Q_{sto2}(t) \quad (11a)$$

$$\frac{dQ_{gut}(t)}{dt} = \eta(P_{eff}) \cdot k_{empt}(Q_{sto}) \cdot Q_{sto2}(t) - k_{abs} \cdot Q_{gut}(t) \quad (11b)$$

Table 7 includes the pramlintide model parameter values and descriptions.

5. Discussion

This paper presents a pramlintide model validated with populational data. The following paragraphs present a series of considerations over each of the model stages, a case study validation integrating the model in a T1D simulator, and a review of the limitations of this work.

The selected model for the intravenous PK stage simplifies the model proposed by Clodi et al. (1998). The three-compartment model has been reduced to a single compartment, providing an adequate description of infusion and bolus data from people with T1D. Of note, the fit for the higher dose (300 μ g) is the least accurate. However, no other works found in the literature use such big intravenous doses for pramlintide therapy. Nevertheless, identified values for physiological parameters are within literature-reported limits: pramlintide distribution volume (V_p) values in the literature range between 14 and 56 l (Colburn et al., 1996; Clodi et al., 1998; Fang et al., 2013) and the identification result provided a value of 31.55 l.

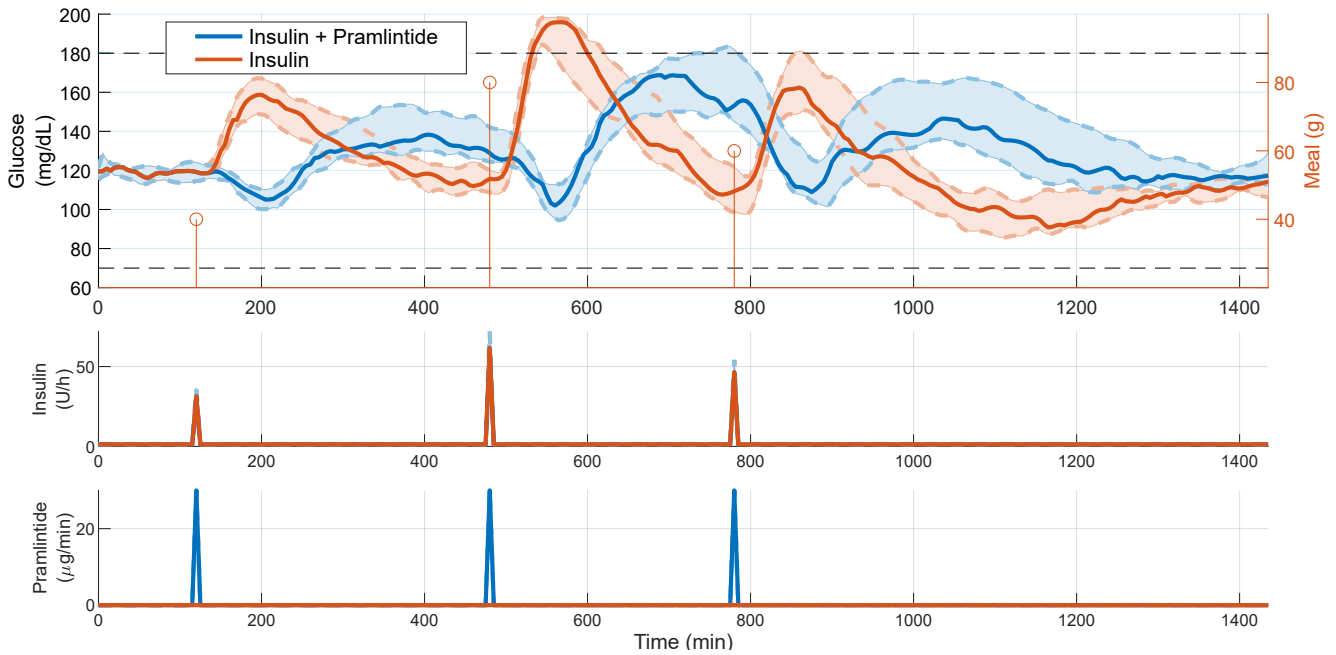


Figure 5: Simulation results after integrating the proposed pramlintide model into the T1D UVA/Padova simulator. Upper graph depicts plasma glucose, middle graph depicts insulin administration, and bottom graph depicts pramlintide administration. Continuous lines represent the mean of the results obtained for the cohort of 10 virtual patients. Shaded areas enclose standard deviation. Results in orange represent a simulation where only insulin was administered (basal infusion and prandial boluses). Results in blue represent a simulation where a 30 μg pramlintide bolus was administered alongside insulin prandial boluses. The simulation scenario consisted of three meals, denoted by circles in the upper graph.

Subcutaneous PK is one of the most relevant stages since most current therapies and clinical trials administer pramlintide subcutaneously. The identified parameters are in the range of the available parameters in the literature. For instance, the bioavailability coefficient identified in this work is around the 40% reported in the Symlin prescribing information (Amylin Pharmaceuticals, 2005). The model's fit to the identification data is accurate (results not shown), but some disparities exist in the fitting of the validation data. Subcutaneous doses of 30 μg were the primary data of interest since the open loop use of pramlintide typically administers a 30 μg bolus alongside meals. In fact, all works used in this paper include at least a 30 μg dose. However, plasma pramlintide data presents some differences across the clinical trials. Most of them report peak plasma pramlintide values between 30 and 40 pmol/l after a 30 μg dose. Conversely, the data from Chase et al. (2009) and Hassan and Heptulla (2009) show plasma values up to 50-60 pmol/l. This magnitude difference could be because the study participants were adolescents instead of adults. The proposed model was fitted with adult aggregated datasets. Therefore, it is reasonable that the model describes the Cha-30 and Has-30 responses more poorly than the other sets (see Figure 2). Hence, to further develop the proposed model, a variety of data from different cohorts would help define these differences.

Regarding the PD stage, the behavior of the two selected datasets (from Woerle et al. (2008) and Hinshaw

et al. (2016)) was rather different. However, even though a single set of parameters could not describe both signals, it was possible to find a single shared model structure. The resulting structure (whose main components are an extra compartment and a Hill equation) allows modulating the shape of the glucose rate of appearance after a meal as a function of the amount of plasma pramlintide. Validation of the effect of pramlintide on gastric emptying using glucose rate of appearance data has an upside and a downside. The positive aspect is that it allows focusing on glucose evolution caused solely by meal ingestion. On the other hand, the glucose rate of appearance is reconstructed based on glucose readings, meaning it is an approximation of the actual signal.

Different parameter sets had to be identified for each dataset used based on the information provided by the placebo arm of the clinical trials. An even more physiologically accurate meal model could have better captured both datasets' behavior. Goyal et al. (2019) stated that the gastric emptying rate depends on the physical characteristics and the caloric density of meals. Focusing on the caloric content, one would expect gastric emptying in the dataset from Hinshaw et al. (2016) to be slower. However, glucose in Woerle et al. (2008) data takes almost 300 minutes to get to half its peak values, whereas, in the former, that time is around 175 minutes. Such a difference does not seem to be explained by meal composition. It could be explained by differences in caloric density (i.e., solids take longer to digest, and liquids leave the stomach faster). Nevertheless,

more data is needed to include this effect in the present model.

The pramlintide proposed model was integrated into an extended version of the UVA/Padova simulator, which implements the glucoregulatory model proposed by Dalla Man (Dalla Man et al., 2014). The objective of this test was to observe whether the addition of the pramlintide model would result in coherent glucose responses after its integration into the T1D simulator. Figure 5 shows the result of a 24-hour simulation for the ten virtual patients available in the simulator. The pramlintide model parameters were maintained the same for the cohort. Specifically, the parameters identified for the Woerle dataset were used (see Table 7). The simulation scenario included three meals (40, 80, and 60 g of carbohydrates). In order to observe the contribution introduced by the pramlintide model, two simulations were carried out with the same scenario: with and without pramlintide (labeled “Insulin + Pramlintide” and “Insulin” in Figure 5, respectively). In the simulation with pramlintide, a 1-min 30 μg pramlintide bolus was administered alongside each meal, as well as an insulin bolus. The simulation shows a delay of the glucose postprandial peak, as well as a reduction of the maximum glucose concentration, similar to the effects reported both in Woerle et al. (2008) and Hinshaw et al. (2016).

Some known physiological effects of amylin were not tested in the model proposed structures due to the data limitations. These effects include the inhibition of glucagon secretion (Lutz, 2022) and the “hypoglycemic override” (Young, 2005). Whereby amylin has no effect in hypoglycemia conditions since hypoglycemia accelerates gastric emptying to raise glucose levels as soon as possible. Another limitation of this work is the use of RMSE as an assessment metric for parameter identification. There was no a priori knowledge about most of the model parameters, which can be troublesome in the identification process.

This study contributes to the study of the pramlintide effect on gastric emptying, building a structured comparison of an incremental model construction based on clinical data results. Despite using aggregated data, the proposed model is simpler than other proposals in the literature, reducing the risk of overfitting. A novel model is proposed that offers an easy-to-implement modulation of the gastric emptying rate as a function of plasma pramlintide concentration. The main limitation is the scarcity of the data used. Without access to complete individual datasets of patients’ data, identifications and validations had to be carried out using aggregated values (similar to Ramkissoon et al. (2014)). Hence, no virtual cohort could be developed. Future work may also improve the parameter identification process, basing the parameter selection on previously defined distributions of the parameters. Nevertheless, the proposed set of parameters describing an average behavior is capable of producing appropriate glucose responses when integrated into a glucoregulatory T1D simulator. This work opens the door to enhancing and improving the proposal with additional dynamics and individual data validation.

Funding

This work was partially supported by: grant FPU17/03404 and PID2019-107722RB-C21 funded by MCIN / AEI / 10.13039/501100011033, grant CIPROM/2021/012 funded by Conselleria de Innovación, Universidades, Ciencia y Sociedad Digital from Generalitat Valenciana.

Acknowledgements

The authors thank Javier Miragall for his preliminary work in defining a pramlintide model and gathering pramlintide datasets, and Borja Pons for data gathering.

References

- Ahrén, B., Adner, N., Svartberg, J., Petrella, E., Holst, J.J., Gutniak, M.K., 2002. Anti-diabetogenic effect of the human letters amylin analogue, pramlintide, in Type 1 diabetes is not mediated by GLP-1. *Diabetic Medicine* 19, 790–792. doi:10.1046/j.1464-5491.2002.00657_1.x.
- Amylin Pharmaceuticals, 2005. Symlin printed labeling (Application number 21-332). Technical Report. URL: https://www.accessdata.fda.gov/drugsatfda_docs/nda/2005/21-332_SymLinInjection_prntlbl.PDF.
- Basu, R., Di Camillo, B., Toffolo, G., Basu, A., Shah, P., Vella, A., Rizza, R., Cobelli, C., 2003. Use of a novel triple-tracer approach to assess postprandial glucose metabolism. *American Journal of Physiology - Endocrinology and Metabolism* 284, 55–69. doi:10.1152/ajpendo.00190.2001.
- Chase, H.P., Lutz, K., Pencek, R., Zhang, B., Porter, L., 2009. Pramlintide Lowered Glucose Excursions and Was Well-Tolerated in Adolescents with Type 1 Diabetes: Results from a Randomized, Single-Blind, Placebo-Controlled, Crossover Study. *Journal of Pediatrics* 155, 369–373. doi:10.1016/j.jpeds.2009.03.012.
- Chiş, O., Banga, J.R., Balsa-Canto, E., 2011. GenSSI: A software toolbox for structural identifiability analysis of biological models. *Bioinformatics* 27, 2610–2611. doi:10.1093/bioinformatics/btr431.
- Clodi, M., Thomaseth, K., Pacini, G., Hermann, K., Kautzky-Willer, A., Waldhäusl, W., Prager, R., Ludvik, B., 1998. Distribution and kinetics of amylin in humans. *American Journal of Physiology - Endocrinology and Metabolism* 274, 903–908. doi:10.1152/ajpendo.1998.274.5.e903.
- Colburn, W.A., Gottlieb, A.B., Koda, J., Kolterman, O.G., 1996. Pharmacokinetics and Pharmacodynamics of AC137 (25,28,29 Tripro-Amylin, Human) After Intravenous Bolus and Infusion Doses in Patients with Insulin-Dependent Diabetes. *The Journal of Clinical Pharmacology* 36, 13–24. doi:10.1002/j.1552-4604.1996.tb04147.x.
- Dalla Man, C., Camilleri, M., Cobelli, C., 2006. A system model of oral glucose absorption: Validation on gold standard data. *IEEE Transactions on Biomedical Engineering* 53, 2472–2478. doi:10.1109/TBME.2006.883792.
- Dalla Man, C., Micheletto, F., Lv, D., Breton, M., Kovatchev, B., Cobelli, C., 2014. The UVA/PADOVA type 1 diabetes simulator: New features. *Journal of Diabetes Science and Technology* 8, 26–34. doi:10.1177/1932296813514502.
- Edelman, S.V., Schroeder, B.E., Frias, J.P., 2007. Pramlintide acetate in the treatment of type 2 and type 1 diabetes mellitus. *Expert Review of Endocrinology and Metabolism* 2, 9–18. doi:10.1586/17446651.2.1.9.
- Faggionato, E., Laurenti, M.C., Vella, A., Man, C.D., 2023. Nonlinear Mixed Effects Modeling of Glucagon Kinetics in Healthy Subjects. *IEEE Transactions on Biomedical Engineering* PP, 1–6. doi:10.1109/TBME.2023.3262974.
- Fang, J., Landersdorfer, C.B., Cirincione, B., Jusko, W.J., 2013. Study Reanalysis Using a Mechanism-Based Pharmacokinetic/Pharmacodynamic Model of Pramlintide in Subjects with Type 1 Diabetes. *The AAPS Journal* 15, 15–29. doi:10.1208/s12248-012-9409-7.
- Gingras, V., Bonato, L., Messier, V., Roy-Fleming, A., Smaoui, M.R., Ladouceur, M., Rabasa-Lhoret, R., 2018. Impact of macronutrient

- content of meals on postprandial glucose control in the context of closed-loop insulin delivery: A randomized cross-over study. *Diabetes, Obesity and Metabolism* 20, 2695–2699. doi:10.1111/dom.13445.
- Goutelle, S., Maurin, M., Rougier, F., Barbaut, X., Bourguignon, L., Ducher, M., Maire, P., 2008. The Hill equation: A review of its capabilities in pharmacological modelling. *Fundamental and Clinical Pharmacology* 22, 633–648. doi:10.1111/j.1472-8206.2008.00633.x.
- Goyal, R.K., Guo, Y., Mashimo, H., 2019. Advances in the physiology of gastric emptying. *Neurogastroenterology and Motility* 31, 1–14. doi:10.1111/nmo.13546.
- Haidar, A., Tsoukas, M.A., Bernier-Twardy, S., Yale, J.F., Rutkowski, J., Bossy, A., Pytko, E., El Fathi, A., Strauss, N., Legault, L., 2020. A novel dual-hormone insulin- and pramlintide artificial pancreas for type 1 diabetes: A randomized controlled crossover trial. *Diabetes Care* 43, 597–606. doi:10.2337/dc19-1922.
- Hassan, K., Heptulla, R.A., 2009. Reducing postprandial hyperglycemia with adjuvant premeal pramlintide and postmeal insulin in children with type 1 diabetes mellitus. *Pediatric Diabetes* 10, 264–268. doi:10.1111/j.1399-5448.2008.00490.x.
- Hay, D.L., Chen, S., Lutz, T.A., Parkes, D.G., Roth, J.D., 2015. Amylin: Pharmacology, Physiology, and Clinical Potential. *Pharmacological Reviews* 67, 564–600. doi:10.1124/pr.115.010629.
- Hinshaw, L., Schiavon, M., Dadlani, V., Mallad, A., Dalla Man, C., Bharucha, A., Basu, R., Geske, J.R., Carter, R.E., Cobelli, C., Basu, A., Kudva, Y.C., 2016. Effect of Pramlintide on Postprandial Glucose Fluxes in Type 1 Diabetes. *The Journal of Clinical Endocrinology and Metabolism* 101, 1954–1962. doi:10.1210/jc.2015-3952.
- Hovorka, R., Canonico, V., Chassin, L.J., Haueter, U., Massi-Benedetti, M., Federici, M.O., Pieber, T.R., Schaller, H.C., Schaupp, L., Vering, T., Wilinska, M.E., 2004. Nonlinear model predictive control of glucose concentration in subjects with type 1 diabetes. *Physiological Measurement* 25, 905–920. doi:10.1088/0967-3334/25/4/010.
- Huffman, D.M., McLean, G.W., Seagrove, M.A., 2009. Continuous subcutaneous pramlintide infusion therapy in patients with type 1 diabetes: observations from a pilot study. *Endocrine practice : official journal of the American College of Endocrinology and the American Association of Clinical Endocrinologists* 15, 689–695. doi:10.4158/EP09044.ORR1.
- Ilkowitz, J.T., Katikaneni, R., Cantwell, M., Ramchandani, N., Heptulla, R.A., 2016. Adjuvant liraglutide and insulin versus insulin monotherapy in the closed-loop system in type 1 diabetes: A randomized open-labeled crossover design trial. *Journal of Diabetes Science and Technology* 10, 1108–1114. doi:10.1177/1932296816647976.
- Kolterman, O.G., Schwartz, S., Corder, C., Levy, B., Klaff, L., Peterson, J., Gottlieb, A., 1996. Effect of 14 days' subcutaneous administration of the human amylin analogue, pramlintide (AC137), on an intravenous insulin challenge and response to a standard liquid meal in patients with IDDM. *Diabetologia* 39, 492–499. doi:10.1007/BF00400683.
- Kong, M.F., King, P., Macdonald, I.A., Stubbs, T.A., Perkins, A.C., Blackshaw, P.E., Moyses, C., Tattersall, R.B., 1997. Infusion of pramlintide, a human amylin analogue, delays gastric emptying in men with IDDM. *Diabetologia* 40, 82–88. doi:10.1007/s001250050646.
- Kong, M.F., Stubbs, T.A., King, P., Macdonald, I.A., Lambourne, J.E., Blackshaw, P.E., Perkins, A.C., Tattersall, R.B., 1998. The effect of single doses of pramlintide on gastric emptying of two meals in men with IDDM. *Diabetologia* 41, 577–583. doi:10.1007/s001250050949.
- Laugesen, C., Ranjan, A.G., Schmidt, S., Nørgaard, K., 2022. Low-Dose Dasiglucagon Versus Oral Glucose for Prevention of Insulin-Induced Hypoglycemia in People With Type 1 Diabetes: A Phase 2, Randomized, Three-Arm Crossover Study. *Diabetes Care* 45, 1391–1399. doi:10.2337/dc21-2304.
- Lutz, T.A., 2022. Creating the amylin story. *Appetite* 172, 105965. doi:10.1016/j.appet.2022.105965.
- Micheletto, F., Dalla Man, C., Kolterman, O., Chiquette, E., Herrmann, K., Schirra, J., Kovatchev, B., Cobelli, C., 2013. In silico design of optimal ratio for co-administration of pramlintide and insulin in type 1 diabetes. *Diabetes Technology and Therapeutics* 15, 802–809. doi:10.1089/dia.2013.0054.
- Miragall, J., Furió-Novejarque, C., Sala-Mira, I., Díez, J.L., Bondia, J., 2023. A new pharmacokinetics and pharmacodynamics model of subcutaneous pramlintide infusion. *Diabetes Technology and Therapeutics* 25, A–136. doi:10.1089/dia.2023.2525.abstracts.
- Müller, T.D., Finan, B., Clemmensen, C., Di Marchi, R.D., Tschöp, M.H., 2017. The new biology and pharmacology of glucagon. *Physiological Reviews* 97, 721–766. doi:10.1152/physrev.00025.2016.
- Paterson, M., Bell, K.J., O'Connell, S.M., Smart, C.E., Shafiq, A., King, B., 2015. The Role of Dietary Protein and Fat in Glycaemic Control in Type 1 Diabetes: Implications for Intensive Diabetes Management. *Current Diabetes Reports* 15, 1–9. doi:10.1007/s11892-015-0630-5.
- Ramkissoon, C.M., Aufderheide, B., Bequette, B.W., Palerm, C.C., 2014. A Model of Glucose-Insulin-Pramlintide Pharmacokinetics and Pharmacodynamics in Type I Diabetes. *Journal of Diabetes Science and Technology* 8, 529–542. doi:10.1177/1932296813517323.
- Rodriguez, L.M., Mason, K.J., Haymond, M.W., Heptulla, R.A., 2007. The role of prandial pramlintide in the treatment of adolescents with type 1 diabetes. *Pediatric Research* 62, 746–749. doi:10.1203/PDR.0b013e318159af8c.
- Rohatgi, A., 2022. WebPlotDigitizer.
- Sherr, J.L., Patel, N.S., Michaud, C.I., Palau-Collazo, M.M., Van Name, M.A., Tamborlane, W.V., Cengiz, E., Carria, L.R., Tichy, E.M., Weinzimer, S.A., 2016. Mitigating meal-related glycemic excursions in an insulin-sparing manner during closed-loop insulin delivery: The beneficial effects of adjunctive pramlintide and liraglutide. *Diabetes Care* 39, 1127–1134. doi:10.2337/dc16-0089.
- van Sloun, B., Goossens, G.H., Erdős, B., O'Donovan, S.D., Singh-Povel, C.M., Geurts, J.M., van Riel, N.A., Arts, I.C., 2023. E-DES-PROT: A novel computational model to describe the effects of amino acids and protein on postprandial glucose and insulin dynamics in humans. *iScience* 26. doi:10.1016/j.isci.2023.106218.
- Taleb, N., Haidar, A., Messier, V., Gingras, V., Legault, L., Rabasa-Lhoret, R., 2017. Glucagon in artificial pancreas systems: Potential benefits and safety profile of future chronic use. *Diabetes, Obesity and Metabolism* 19, 13–23. doi:10.1111/dom.12789.
- Thompson, R.G., Peterson, J., Gottlieb, A., Mullane, J., 1996. Effects of Pramlintide, an Analog of Human Amylin, on Plasma Glucose Profiles in Patients With IDDM: Results of a Multicenter Trial.
- Tsoukas, M.A., Cohen, E., Legault, L., von Oettingen, J.E., Yale, J.F., Vallis, M., Odabassian, M., El Fathi, A., Rutkowski, J., Jafar, A., Ghanbari, M., Gouchie-Provencher, N., René, J., Palisaitis, E., Haidar, A., 2021a. Alleviating carbohydrate counting with a FiASP-plus-pramlintide closed-loop delivery system (artificial pancreas): Feasibility and pilot studies. *Diabetes, Obesity and Metabolism* 23, 2090–2098. doi:10.1111/dom.14447.
- Tsoukas, M.A., Majdpour, D., Yale, J.F., Fathi, A.E., Garfield, N., Rutkowski, J., Rene, J., Legault, L., Haidar, A., 2021b. A fully artificial pancreas versus a hybrid artificial pancreas for type 1 diabetes: a single-centre, open-label, randomised controlled, crossover, non-inferiority trial. *The Lancet Digital Health* 3, e723–e732. doi:10.1016/S2589-7500(21)00139-4.
- Walter, E., Lecourtier, Y., 1982. Global approaches to identifiability testing for linear and nonlinear state space models. *Mathematics and Computers in Simulation* 24, 472–482. doi:10.1016/0378-4754(82)90645-0.
- Weinzimer, S.A., Sherr, J.L., Cengiz, E., Kim, G., Ruiz, J.L., Carria, L., Voskanyan, G., Roy, A., Tamborlane, W.V., 2012. Effect of pramlintide on prandial glycemic excursions during closed-loop control in adolescents and young adults with type 1 diabetes. *Diabetes Care* 35, 1994–1999. doi:10.2337/dc12-0330.
- Weyer, C., Gottlieb, A., Kim, D.D., Lutz, K., Schwartz, S., Gutierrez, M., Wang, Y., Ruggles, J.A., Kolterman, O.G., Maggs, D.G., 2003. Pramlintide Reduces Postprandial Glucose Excursions When Added to Regular Insulin or Insulin Lispro in Subjects With Type 1 Diabetes. *Diabetes Care* 26, 3074–3079. doi:10.2337/diacare.26.11.3074.
- Weyer, C., Maggs, D., Young, A., Kolterman, O., 2001. Amylin Replacement With Pramlintide as an Adjunct to Insulin Therapy in Type 1 and Type 2 Diabetes Mellitus: A Physiological Approach Toward

Table 8

Pramlintide intravenous pharmacokinetics AIC and BIC results for validation STAGE-IV1, validation STAGE-IV2, and identification results of STAGE-IV3. The section “Combination of STAGE-IV1 and STAGE-IV2” presents the metric results obtained to select the model structures used in STAGE-IV3. The expressions of $\bar{\mu}$ and \bar{M} are defined in Equation (7). The highlighted value in each row represents the lowest value.

	Intravenous PK model structures					
STAGE-IV1	1	1A	2	2A	3	3A
Mean AIC	74.30	94.93	70.18	89.37	66.20	97.95
Median AIC	65.69	88.78	61.32	82.64	57.41	96.50
Mean BIC	75.21	96.32	70.12	89.80	65.17	97.41
Median BIC	66.60	90.17	61.26	83.06	56.38	95.96
STAGE-IV2	1	1A	2	2A	3	3A
Mean AIC	152.64	132.72	138.96	130.74	131.09	123.23
Median AIC	152.42	122.16	137.37	121.26	129.74	117.17
Mean BIC	153.55	134.12	138.90	131.16	130.06	122.69
Median BIC	153.33	123.55	137.31	121.69	128.71	116.62
Combination of STAGE-IV1 and STAGE-IV2	1	1A	2	2A	3	3A
$\bar{\mu}_{AIC}$	113.47	113.83	104.57	110.06	98.65	110.59
\bar{M}_{AIC}	109.06	105.47	99.35	101.95	93.57	106.84
$\bar{\mu}_{BIC}$	114.38	115.22	104.51	110.48	97.62	110.05
\bar{M}_{BIC}	109.97	106.86	99.28	102.37	92.54	106.29
STAGE-IV3	2	2A	3			
Mean AIC	97.86	94.86	94.37			
Median AIC	100.40	102.19	96.33			
Mean BIC	97.80	95.29	93.34			
Median BIC	100.34	102.61	95.30			

Improved Metabolic Control. *Current Pharmaceutical Design* 7, 1353–1373. doi:10.2174/1381612013397357.

Wilinska, M.E., Chassin, L.J., Schaller, H.C., Schaupp, L., Pieber, T.R., Hovorka, R., 2005. Insulin kinetics in type-1 diabetes: Continuous and bolus delivery of rapid acting insulin. *IEEE Transactions on Biomedical Engineering* 52, 3–12. doi:10.1109/TBME.2004.839639.

Wilson, L.M., Jacobs, P.G., Castle, J.R., 2020. Role of Glucagon in Automated Insulin Delivery. *Endocrinology and Metabolism Clinics of North America* 49, 179–202. doi:10.1016/j.ecl.2019.10.008.

Woerle, H.J., Albrecht, M., Linke, R., Zschau, S., Neumann, C., Nicolaus, M., Gerich, J.E., Göke, B., Schirra, J., 2008. Impaired hyperglycemia-induced delay in gastric emptying in patients with type 1 diabetes deficient for islet amyloid polypeptide. *Diabetes Care* 31, 2325–2331. doi:10.2337/dc07-2446.

Young, A., 2005. Inhibition of Gastric Emptying. *Advances in Pharmacology* 52, 99–121. doi:10.1016/S1054-3589(05)52006-4.

B. Data availability

The data that support the findings of this study are available from the corresponding author, J.B., upon request.

A. AIC and BIC validation results

This section includes the AIC and BIC values of the validation process for the intravenous pharmacokinetics stage (Table 8), the subcutaneous pharmacokinetics stage (Table 9), and the identification results of the pharmacodynamics stage (Table 10). For more information about each stage refer to Table 2.

Table 9

Pramlintide subcutaneous pharmacokinetics AIC and BIC results for STAGE-SC validation, with each of the selected IV structures (2, 2A, and 3). The highlighted value in each row represents the lowest value.

		Subcutaneous PK model structures							
STAGE-SC (IV model 2)		1	1A	2	2A	3	3A	4	4A
Mean AIC		53.47	50.50	55.56	47.58	43.91	43.33	45.91	48.00
Median AIC		50.58	49.42	52.78	46.71	46.46	48.50	48.43	50.42
Mean BIC		53.18	50.15	55.22	47.18	43.51	42.87	45.45	47.48
Median BIC		50.26	48.63	52.39	46.14	45.54	47.45	47.38	49.24
STAGE-SC (IV model 2A)		1	1A	2	2A	3	3A	4	4A
Mean AIC		55.37	52.21	57.48	46.99	43.84	45.28	45.82	47.03
Median AIC		52.07	51.17	54.19	48.40	48.34	50.40	50.35	52.66
Mean BIC		55.02	51.81	57.07	46.53	43.38	44.76	45.30	46.45
Median BIC		51.68	50.25	53.73	47.35	47.30	49.22	49.17	51.35
STAGE-SC (IV model 3)		1	1A	2	2A	3	3A	4	4A
Mean AIC		49.43	46.47	51.53	44.06	39.85	39.36	41.90	41.48
Median AIC		46.60	45.40	48.79	43.15	42.45	44.44	44.44	46.47
Mean BIC		49.25	46.24	51.30	43.77	39.56	39.01	41.56	41.08
Median BIC		46.41	44.88	48.54	42.88	41.80	43.65	43.66	45.55

Table 10

Pramlintide subcutaneous pharmacodynamics AIC and BIC results. The highlighted value in each row represents the lowest value.

		PD model structures											
STAGE-PD1		1A	1B	1C	1D	2A	2B	2C	2D	3A	3B	3C	3D
AIC		12.31	-13.70	-11.69	-36.18	10.20	-11.71	-9.70	-38.51	-11.70	-9.71	-7.69	-35.93
BIC		11.01	-14.99	-12.28	-36.06	8.91	-12.29	-9.57	-37.68	-12.29	-9.58	-6.86	-34.38
STAGE-PD2		1A	1B	1C	1D	2A	2B	2C	2D	3A	3B	3C	3D
AIC		46.49	17.72	7.45	-9.64	44.10	19.93	9.38	-8.05	7.32	9.32	11.33	-5.96
BIC		45.32	16.55	7.12	-9.14	42.93	19.59	9.88	-6.72	6.98	9.82	12.66	-3.79